Reorientational Jump Dynamics and Its Connections to Hydrogen Bond Relaxation in Molten Acetamide: An All-Atom Molecular Dynamics Simulation Study

ARTICLE *in* THE JOURNAL OF PHYSICAL CHEMISTRY B · DECEMBER 2014

Impact Factor: 3.3 · DOI: 10.1021/jp509869d · Source: PubMed

3 AUTHORS:

Suman Das
S N BOSE NATIONAL CENTRE FOR BASIC SCIE…
5 PUBLICATIONS **43** CITATIONS
SEE PROFILE

Ranjit Biswas
S.N. Bose National Centre for Basic Sciences
99 PUBLICATIONS **1,823** CITATIONS
SEE PROFILE

Biswaroop Mukherjee
S.N. Bose National Centre for Basic Sciences
15 PUBLICATIONS **227** CITATIONS
SEE PROFILE

THE JOURNAL OF PHYSICAL CHEMISTRY B

Article

pubs.acs.org/JPCB

Reorientational Jump Dynamics and Its Connections to Hydrogen Bond Relaxation in Molten Acetamide: An All-Atom Molecular Dynamics Simulation Study

Suman Das,[†] Ranjit Biswas,*[,†,‡] and Biswaroop Mukherjee*[,‡]

[†]Chemical, Biological and Macromolecular Sciences, and [‡]Thematic Unit for Excellence−Computational Materials Science, S. N. Bose National Centre for Basic Sciences, Block-JD, Sector-III, Salt Lake, Kolkata, 700098, India

Supporting Information

ABSTRACT: Here we report results from our molecular dynamics simulations on orientational relaxation and hydrogen bond dynamics of molten acetamide. Signatures for orientational jumps have been detected with jump barrier estimated to be ∼0.7 k_BT. Simulated orientational relaxations indicate deviations from hydrodynamics and this deviation has been ascribed to the detected orientational jumps. Simulated free energy surfaces obtained at various distances between the rotating acetamide and its initial and final H-bond acceptors have been found to be symmetric double-well in nature at the transition state. H-bond relaxation times obtained from our simulations corroborate well with the time scales associated with the jump and waiting time distributions, suggesting an interrelationship between jump dynamics and H-bond fluctuations. Jump angle distributions are asymmetric and depict long tails extending to large angles.

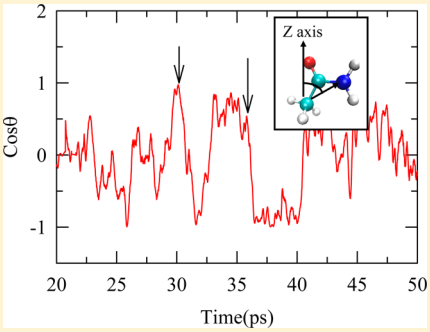

I. INTRODUCTION

The presence of a peptide bond (−OC−NH−) and its occurrence as a repeat unit in polypeptides and proteins have rendered biological relevance to acetamide (CH_3CONH_2) .[1,2] In addition, the ability of CH_3CONH_2 to participate in hydrogen bonding (H-bonding) has made this molecule as an excellent model system for studying the role of H-bonding interactions in determining the three-dimensional structures of proteins and nucleic acids.[3−5] The presence of methyl, carbonyl, tautomeric hydroxyl, and amide groups in the same molecule has made acetamide an excellent solvent for a very large number of organic and inorganic substances.[6,7] Interestingly, the high static dielectric constant ($\varepsilon_0 \sim 60$) of molten acetamide (melting temperature ∼ 350 K, and viscosity ∼ 2.2 cP) coupled with its large dipole moment (3.7 D) have made acetamide an even better solvent than water for many ionic compounds.[6−10] As a result, interaction and dynamics in acetamide and other simpler amides have been the subject of a large number of studies.[11−18] Of late, deep eutectic solvent (DES) systems containing acetamide have been studied using fast spectroscopic techniques and computer simulations in order to explore the interrelationship between solution structure and dynamics of these room temperature molten mixtures.[19−25] The utility of these DES systems as cheap replacements for ionic liquids as reaction media in chemical industries,[26,27] and the application aspect of controlling reactions via understanding the relationship between dynamic solvent response and reaction rate[28,29] in such media have further motivated research in this direction. Although the above combined spectroscopic and simulation studies have revealed some structural and dynamical aspects of acetamide in the presence of electrolytes, a similar investigation for neat liquid acetamide is still unavailable and thus warrants an in-depth study.

In this paper, we have performed all-atom molecular dynamics simulations to study the orientational relaxation of neat liquid acetamide at 368 K and investigate whether orientational jumps, as in the case of liquid water,[30−35] contribute substantially to the collective orientational relaxation. The interconnection between H-bond dynamics[36−42] of molten acetamide at this temperature and orientation jumps have been explored. In addition, the coupling between translation and rotation in neat liquid acetamide has been investigated. Both the simulated acetamide backbone and N−H vector orientational relaxations suggest presence of non-hydrodynamic reorientation mechanism. The presence of orientational jumps is revealed when the cosine of the angle made by the acetamide backbone with the Z-axis of the simulation box is followed over time. A broad distribution for the jump angle has been found along with a significant center-of-mass displacement (∼25−50% of acetamide diameter) during a jump of as large as 90°. Simulated waiting time (between two successive jumps) and jump time distributions have been found to be exponential at long time with the mean waiting time ∼2.5 times longer than the mean jump time. As expected, the continuous H-bond lifetime has been found to be shorter than the jump time. The free energy barrier associated with orientation jumps has been found to be ∼0.7 k_BT which is

Received: September 30, 2014
Revised: November 23, 2014
Published: December 11, 2014

DOI: 10.1021/jp509869d
J. Phys. Chem. B 2015, 119, 274−283

approximately one-fourth of that reported[30,31] for neat liquid water. The essential feature of this reorientation mechanism is the coupling between the orientation and the concerted center-of-mass motion of the triad of molecules participating in the microscopic orientational jump. This feature is also shared by liquid water,[30,31] making this translation−rotation coupling a universal feature of all H-bonded liquids.

II. SIMULATION DETAILS

All-atom molecular dynamics simulations were performed using 256 CH_3CONH_2 molecules at 368 K (CH_3CONH_2 melts at ∼350 K)[43] with DL_POLY version 2.20,[44] where the molecules interacted via the following potential function:[45]

$$U(R) = \sum_{\text{bonds}} K_r(r - r_{\text{eq}})^2 + \sum_{\text{angles}} K_\theta(\theta - \theta_{\text{eq}})^2 + \sum_{\text{dihedrals}} K_\varphi[1 + \cos(n\varphi - \delta)] + \sum_{i<j}^{\text{atoms}} \left(\frac{A_{ij}}{R_{ij}^{12}} - \frac{B_{ij}}{R_{ij}^{6}}\right) + \sum_{i<j}^{\text{atoms}} \frac{q_i q_j}{4\pi\varepsilon_0 R_{ij}} \quad (1)$$

In eq 1, K_r is the bond constant with the equilibrium bond distance r_{eq}, K_θ is the angle constant with the equilibrium angle θ_{eq}, K_ϕ is the dihedral constant with periodicity n, dihedral angle ϕ and phase shift δ. R_{ij} is the distance between atoms i and j with partial charges q_i and q_j, respectively. The interaction parameters for the acetamide molecule were taken from the CHARMM[46] force field and summarized in the Supporting Information. The force field was constructed using DL_FIELD.[47] Such a construction was found earlier to generate a reasonable description of acetamide dynamics in molten mixtures.[21,22] The short-range van der Waals interaction was represented by the Lennard-Jones (LJ) potential, and the long-range electrostatic potential was treated via Ewald summation technique[48] using an Ewald parameter of α = 0.2 Å^{-1} and a 6 × 6 × 6 k-point grid.

The initial configuration was built using Packmol[49] and equilibrated in NPT ensemble at 1 atm. pressure for 500 ps. Fidelity of the simulations was then checked by reproducing the experimental density (1.16 g/cm^3)[50] at 353 K. Nose−Hoover thermostat[51] and barostat[52] were used to control the temperature and pressure with time constant of 0.5 and 1.0 ps, respectively. Subsequently, further equilibration of 1 ns followed by a production run of 5 ns was carried out in *NVT* ensemble. Periodic boundary conditions were employed in all three directions, and the equations of motion were integrated using a time step of 0.5 fs employing the velocity Verlet algorithm.[48] Snapshots were saved every 10 fs for data analyses and simulation results. Note that the simulations were carried out at 368 K in order to completely avoid complexities arising from being in close proximity to the melting temperature (∼350 K).

III. ANALYSIS PROTOCOL

Figure 1 displays the time series of the cosine of the angle made by the backbone of a randomly chosen CH_3CONH_2 molecule (connecting the C (−CH_3) and N(−NH_2) atom) with the Z axis of the simulation box. Clearly, the chosen CH_3CONH_2 molecule executes diffusive reorientation as well as angular jumps, with jump amplitude sometimes as large as 90°. Such features (diffusive reorientation punctuated by large amplitude angular jumps) are strongly reminiscent of the reorientation mechanism in liquid water.[30,31,53] We have analyzed microscopic trajectories generated from MD simulations for uncovering the details of the reorientation mechanism in molten acetamide.

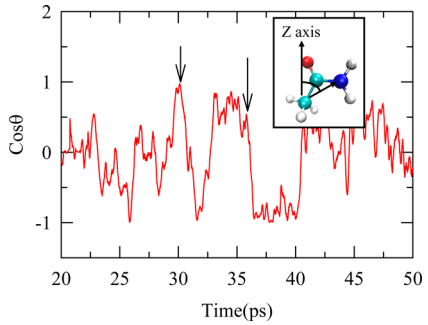

Figure 1. Plot shows the time series of the cosine of the angle which the backbone of a randomly chosen acetamide molecule makes with the Z axis of the simulation box. The reorientational dynamics exhibits diffusive reorientation as well as large amplitude orientational jumps (indicated by arrows).

A large amplitude angular jump involves a change in the hydrogen bond (H-bond) partners of the molecule in question. Prerequisite for such an identification is the knowledge of H-bond partners of a molecule in a given simulation snapshot. H-bonds can be defined in a number of ways based on geometric criteria, energy consideration or orbital occupancy.[32] Here, we have chosen a widely accepted geometric definition based on a distance (R) and an angle (deg). Two CH_3CONH_2 molecules are considered to be H-bonded if the following criteria are satisfied: (i) the distance between the oxygen and nitrogen atoms belonging to different CH_3CONH_2 molecules, R_{ON}, is less than a cutoff distance, R_{cutoff}, and (ii) the angle between the vector joining nitrogen and amide hydrogen of one CH_3CONH_2 molecule and the vector joining this nitrogen and an oxygen atom belonging to another acetamide molecule, θ_{ONH}, is less than 30°. R_{cutoff} is taken as the distance at which appears the first minimum of the simulated radial distribution function ($g_{ON}(r)$) for the oxygen and the nitrogen atoms belonging to different CH_3CONH_2 molecules. In our simulations at 368 K, this has been found to be 4 Å, as shown in Figure 2. Note that the first peak of the simulated $g_{ON}(r)$ occurs at ∼3 Å, which agrees well with the results from X-ray scattering measurements of CH_3CONH_2.[11,12] This

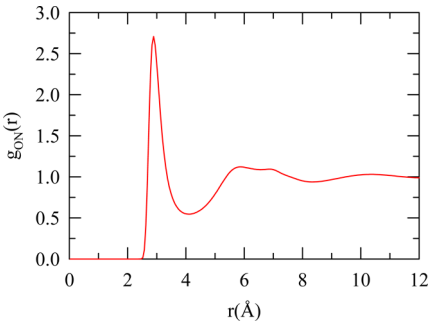

Figure 2. Radial distribution function, $g_{ON}(r)$, between the oxygen and the nitrogen atoms belonging to two different acetamide molecules. The cutoff distance (for the hydrogen bond definition) is taken at 4 Å, which corresponds to the first minima of the above $g_{ON}(r)$, and it measures the extent of the first solvation shell.

DOI: 10.1021/jp509869d
J. Phys. Chem. B 2015, 119, 274−283

agreement between simulations and experiments suggests the validity of the interaction potential used.

Since the criterion we have used for determining whether pairs of molecules are hydrogen bonded or not is somewhat arbitrary (R_{ON} < 4 Å and θ_{ONH} < 30°), we decided to impose another H-bonding criterion for making our study robust. First, we search for pairs of molecules for which the distance between the nitrogen and oxygen, R_{ON} is less than 4 Å. Then we monitor the distance between the hydrogen atoms and oxygen atom for these pairs of molecules. The distribution, shown in Figure 3, is double peaked for the two hydrogen atoms of the

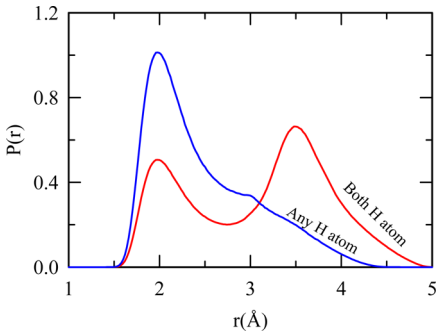

Figure 3. Distance distributions between hydrogen and oxygen atoms of a pair of nearby acetamide molecules. Modified hydrogen bond criteria is derived by choosing the cutoff distance between oxygen and hydrogen at 2.5 Å. Double peak (red curve) structure is obtained when the locations of both the amide H atoms (with respect to the oxygen atom of another participating acetamide molecule) are monitored. Monitoring of only the nearest H atom leads to the blue curve possessing a peak and a shoulder.

chosen acetamide molecule, signifying the most probable locations of them with respect to the oxygen atom of a neighboring acetamide molecule. The probability distribution for any of the two H atoms which are at the nearest distance to the oxygen (of the neighboring acetamide) is also shown in Figure 3. Considering these two distributions, we have chosen a cutoff distance between O and H atoms of hydrogen-bonded pairs of acetamide molecules as 2.5 Å. This cutoff distance of 2.5 Å correlates well with the hydrogen bond distance for N−H···O moiety estimated from X-ray and neutron diffraction measurements of a large number organic crystals possessing such an interaction.[54] With this added H-bonding criteria, we have evaluated the waiting time distribution, which is sensitive to the definition of H-bond. Note this additional H-bond criterion has not altered the qualitative feature of the waiting time distribution (shown later) but induced a small change (∼10−15%) in the numerical value of the mean waiting time. As a result, we stick to our first definition of H-bond for the rest of the calculations.

Considering the first definition of H-bonding we have identified the H-bond switching events as follows. Two flags have been associated with each CH_3CONH_2 molecule, flag_H1(i,t) and flag_H2(i,t). Here "i" denotes the index of the CH_3CONH_2 molecule and "t" the label for the simulation snapshot. The value of a flag of molecule "i", if nonzero, denotes the index of the acetamide molecule H-bonded to the "i"th molecule. If its value is zero, it means that the particular hydrogen of molecule "i" is not H-bonded to any other acetamide molecule. The two flags thus represent the H-bonding state of the two H atoms of the $-NH_2$ group since both H atoms are capable of forming H-bonds. Figure 4a shows a typical microscopic process extracted from our simulations,

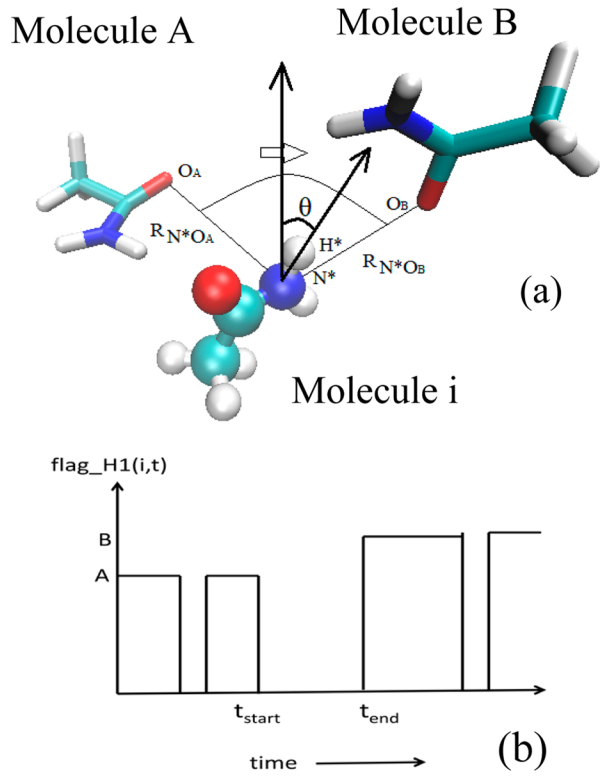

Figure 4. Top panel: Intermediate configuration while an orientational jump occurs. The N*H* vector of the rotating molecule (shown in ball and stick representation) is initially bonded to oxygen atom O_A of molecule A. It breaks this hydrogen bond and then simultaneously orients and then forms a hydrogen bond to atom O_B of molecule B. Bottom panel: How the above process can be represented by the change in the value of a flag variable, which is defined in the text. This flag variable has a value of A (the index of the molecule to which it is hydrogen bonded to) initially, later, it attains a value of B (new hydrogen bonding partner). The times at which the jump starts and ends are also identified.

where the rotating molecule (in ball-and-stick representation) performs a large amplitude angular jump. It was initially H-bonded to molecule "A", and it breaks this bond and rotates and forms a new H-bond with molecule "B". Such a microscopic process can be translated to time-dependence of the flag variables. Figure 4b shows the same process in terms of the flag variables. The variable flag_H1(i,t) initially has a nonzero value equal to "A", which denotes that the rotating molecule "i" is H-bonded to molecule "A". Note that the H-bond between "i" and "A" can break temporarily and then re-form, which is signified by the value of the flag jumping discontinuously from "A" to zero and back to "A". These are examples of temporal H-bond fluctuations and do not involve large amplitude angular jumps. The events that we are interested in identifying are the ones where the identity of the H-bonding partners changes resulting in a large orientational displacement. The "start" time (t_{start} in Figure 4b) is the last instant when molecule "i" was H-bonded to its initial partner "A". Similarly, the end-time, t_{end}, is the first instant when molecule "i" forms a H-bond with its final partner molecule "B".

DOI: 10.1021/jp509869d
J. Phys. Chem. B 2015, 119, 274−283

Subsequently, we construct a time series of flag_H1(i,t) and flag_H2(i,t) for all molecules at all instants during the production run. From such time series, we identify all t_{start} and t_{end} where the microscopic jumps start and end. The identification of these times allows us to calculate the distributions of the waiting time between jumps and the distribution of the time required to complete the jumps. We then compare the time scales associated with these distributions with those obtained from the simulated H-bond time correlation functions. The knowledge of the start and end times also allows us to calculate the orientational displacement of the molecules during these times. The transition state of the orientational jump occurs when $R_{N^*O_A}$ equals $R_{N^*O_B}$ (see Figure 4a for these geometrical definitions). For each microscopic jump, we search between times t_{start} and t_{end} when $R_{N^*O_A}$ becomes equal to $R_{N^*O_B}$. For this we numerically estimate the minimum value of the modulus of $(R_{N^*O_A} - R_{N^*O_B})$. The value of the angle $O_AN^*O_B$ at the transition state is a good descriptor of the jump angle of the rotating N*−H* vector. This choice may seem odd, but this is the only way one can remove the effects arising from the librational motion of the N*−H* vector of the rotating acetamide molecule. Naively one may consider that the angular displacement can be estimated easily by calculating the angular displacement of the N*−H* vector of the rotating acetamide molecule in the time interval between t_{start} and t_{end}. This is incorrect as this does not exclude the error arising from the librational motion of the rotating N*−H* vector, which can be significant compared to the jump angle that one wants to determine. However, in the case of orientational displacement of the backbone, where the effects of libration are minimal, we have followed this simpler method.

For the calculation of the average trajectory, we choose jumps in the following way: a single molecule can perform several orientational jumps within the simulation time window. Once the transition times for all jumps of a particular molecule are known, we choose those jumps whose transitions times differ by more than 340 fs, with the transition time at the center of this time window (170 fs preceding and 170 fs following the transition time). This time interval (170 fs) has been decided by monitoring whether the distances and angles reach their corresponding saturation values at the beginning and end of the average trajectories. We ensure that within this 340 fs interval the particular molecule does not participate in any other hydrogen bond switching event apart from the chosen one. We do this for all the molecules in the system and finally a "coherent average" is taken for all the relevant geometrical quantities defining the microscopic trajectory. During the "coherent averaging", the transition state is chosen as the origin of time at the center of the average trajectory with the jump starting at −170 fs and ending at +170 fs. In this fashion where one coincides the transition times of all the microscopic trajectories considered ("coherent averaging"), one can extract generic features from microscopic trajectories, without the important features being swamped by the presence of inherent thermal fluctuations. The geometrical quantities for which the "average" temporal dependence are calculated are distances $R_{N^*O_A}$, $R_{N^*O_B}$ and the angle formed by the projection of the N*−H* vector on the $O_AN^*O_B$ plane and the angle bisector of angle $O_AN^*O_B$ (see Figure 4a for these geometrical definitions). These distances and angles describing the average trajectory have been obtained by coherent averaging over microscopic trajectories exhibiting H-bond jumps.

Finally, we have estimated the free energy barrier associated with an average reorientational trajectory. Following the method devised earlier for liquid water,[30,31] we construct a three-dimensional free energy profile, which depends on the difference of the H-bond coordination numbers of initial donor and final donor, Δn_{HB}, the difference in the distance between N* (N atom belonging to the rotating CH_3CONH_2 molecule) and O_A (O atom belonging to the initial H-bond acceptor), and N* and O_B (O atom belonging to the final H-bond acceptor), ΔR, and one angular coordinate θ (defined in Figure 4a). A probability distribution function (histogram), $P(\Delta n_{HB}, \Delta R, \theta)$ was first calculated based on these three coordinates. This calculation proceeds in the following way: Refer to Figure 5,

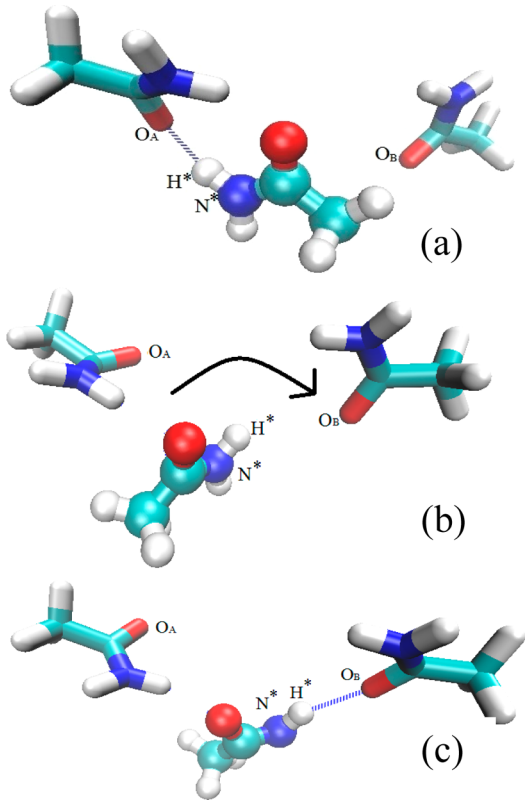

Figure 5. Orientational jump mechanism in liquid acetamide: the vector N*−H* undergoes a orientational jump. Initially it is hydrogen bonded to oxygen O_A (panel a), which belongs to acetamide A, it breaks the hydrogen bond (panel b), and it finally forms a new hydrogen bond with oxygen O_B, belonging to acetamide B (panel c).

which shows a typical jump event whose t_{start} and t_{end} have been identified by the above protocol. The nitrogen atom of the rotating CH_3CONH_2 molecule is denoted by N* and N*−H* vector is initially H-bonded to the oxygen atom O_A of the neighboring molecule. During the jump, this H-bond breaks and the molecule rotates and N*−H* forms a H-bond with atom O_B of another CH_3CONH_2 in the vicinity of the rotating neighbor. Suppose this is the j^{th} orientational jump of the chosen molecule and its t_{start} and t_{end} are denoted by $t_{start}(j)$ and $t_{end}(j)$. We calculate the contributions to the probability distribution function, $P(\Delta n_{HB}, \Delta R, \theta)$ only during three types of time intervals: (i) $t_{end}(j-1) < t < t_{start}(j)$, (ii) $t_{start}(j) < t < t_{end}(j)$, and (iii) $t_{end}(j) < t < t_{start}(j+1)$. During these intervals

DOI: 10.1021/jp509869d
J. Phys. Chem. B 2015, 119, 274−283

we calculate the value of the variables $\Delta n_{HB,}$ ΔR, and θ from the microscopic MD trajectories and construct a histogram by binning them. The sizes of the bins used in this calculation are ΔR = 0.1 Å, Δn = 1, and $\Delta\theta$ = 3°.

Contributions arising from interval i contribute to the initial free energy minima (on the reactant side, these orientational jumps can also be viewed as a chemical reaction[30,31] even though in this case only migration of hydrogen bonds, rather than formation and breakage of covalent bonds, is involved). Contributions from interval ii contribute to the regions around the transition state of this reaction, and contributions from interval iii contribute to the final free energy minima (product side of the reaction). This procedure is then followed for all the molecules in the system to yield the probability distribution function, $P(\Delta n_{HB}, \Delta R,\theta)$. Finally the free energy $G(\Delta n_{HB}, \Delta R,\theta)$ is determined using the following expression,

$$G(\Delta n_{HB}, \Delta R, \theta) = -k_B T \ln[P(\Delta n_{HB,}\Delta R, \theta)]) \quad (2)$$

This calculation protocol ensures that the prediction of the free energy surface and its sections are symmetric with respect to the reactant and product states.

IV. RESULTS AND DISCUSSION

Figure 6 shows the time-evolution of $R_{N^*O_A}$ and $R_{N^*O_B}$ with time during an average H-bond switching event. The behavior of the average trajectory shows that the molecule containing atom O_A moves from the first coordination shell to the second coordination shell whereas, the molecule containing atom O_B moves in from the second coordination to the first. The coordination shells can be identified from the radial distribution function between the oxygen and nitrogen atoms belonging to different CH_3CONH_2 molecules (see Figure 2). As in the case of liquid water, the role played by the translational motion of amide O_A and O_B is very important, and the symmetric configuration when both $R_{N^*O_A}$ and $R_{N^*O_B}$ are equal is the transition state.[30,31] The magnitude of translational displacement of the oxygen atoms of the initial and final H-bond acceptors during the "average" orientational jump is ~2 Å. The bottom panel of Figure 6 shows that the average trajectory of the angle formed by the projection of the N*−H* vector on the $O_AN^*O_B$ plane and the angle bisector of angle $O_AN^*O_B$. This average angle exhibits a sharp transition from an angle of −45° to +45°, signifying a jump of about 90°. This angle is zero at the transition state and is negative before the transition state and positive after it crosses the transition state.

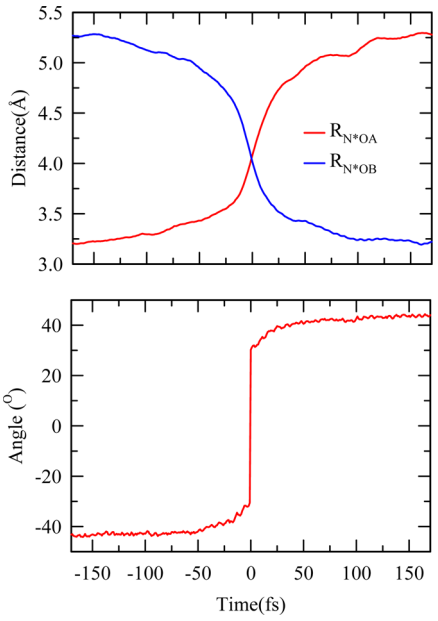

Figure 6. Top panel: Time evolution of the distances $R_{N^*O_A}$ (red curve) and $R_{N^*O_B}$ (blue curve), calculated for the average jump trajectory. The oxygen of the initial acceptor, moves out from the first solvation shell to the second solvation shell, whereas the final acceptor moves in from the second to the first shell. The solvation shells are evident from the radial distribution function (see Figure 2) between the oxygen atom and the nitrogen atom belonging to two different acetamide molecules. Bottom panel: How angle θ (defined in Figure 4a) varies in an average trajectory. It jumps from a value of −45° to +45°, showing a jump of about 90°.

In order to estimate the effects these orientational jumps have on the center-of-mass (COM) coordinates, we have recalculated the above average trajectories using the COM coordinates of the triad of molecules (the rotating molecule, the initial and the final H-bond acceptors). O_A, N*, and O_B have been replaced by the COM of the three chosen molecules. Figure 7 shows the average trajectory calculated using the center of mass coordinates, the definition of the angle also changes similarly. The translational displacement associated with the average orientational jump is ~0.8 Å in a time interval of 340 fs (the extent of the time axis in Figure 7). One can estimate the value of translational diffusion coefficient (D_T) of liquid acetamide from the Stokes−Einstein relation,[55] $D_T = k_BT/4\pi\eta r$, k_BT being the Boltzmann constant times the absolute temperature and r the radius of the diffusing molecule. Using a value of viscosity[23] ($\eta \sim 2$ cP) and $r \sim 2$ Å, we find $D_T \sim 10 \times 10^{-5}$ Å^2/fs. The diffusive displacement estimated from the relation,[55] $\Delta r^2 = 6D_Tt$, turns out to be $\Delta r \sim 0.4$ Å in 340 fs. In reality (in the presence of orientational jumps) the

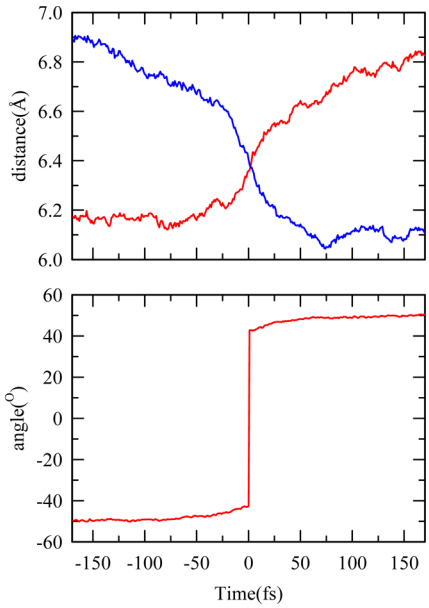

Figure 7. Average trajectory calculated in terms of the distance between center-of-mass (COM) of the rotating acetamide and its initial (red curve) and final (blue curve) H-bond acceptors (top panel). The bottom panel shows how angle θ (defined in Figure 4a) varies in an average trajectory. For further discussion, see text.

DOI: 10.1021/jp509869d
J. Phys. Chem. B 2015, 119, 274−283

magnitude of COM translational displacement is ∼0.8 Å (see the upper panel of Figure 7) which is nearly double the value of Δr. This COM displacement and the translational displacement of the oxygen atom displayed in Figure 6 (∼2 Å) jointly suggest that the translational motion of the nitrogen and oxygen atoms is significantly influenced by the orientational jumps. This shows the natural coupling which is always present between translational and orientational modes in such complex systems.

Figure 8 (main panel) demonstrates the jump angle distribution calculated from the orientational displacements of

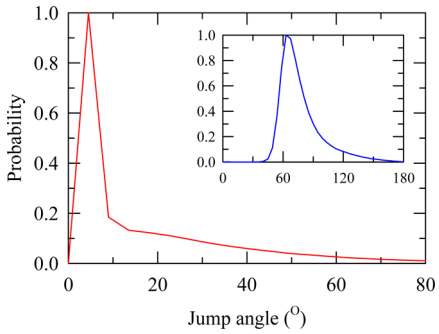

Figure 8. Jump angle distributions for acetamide at 368 K from simulations. Main panel shows the jump angle distribution for the backbone of the acetamide molecule, whereas the inset presents the jump angle distribution of the N*−H* vector, which participates in the exchange of the hydrogen-bonding partner.

the backbone of the acetamide molecules between the starting and ending times of the microscopic jumps. The curve peaks at around 5° but displays a long tail extending toward larger jump angles. A more magnified view of the jump angle distribution can be accessed via considering the angular motion of the N*−H* vector. The jump angle, in such a description, is the angle $O_AN^*O_B$ at the transition state when $R_{N^*O_A} = R_{N^*O_B}$ (see Figure 4(a)). Inset of Figure 8 shows this distribution which peaks at ∼60° and again displays a long tail extending to large angles. This clearly indicates that large amplitude jumps are associated with angular dynamics of the N*−H* vector. This means that the N*−H* vector probably first undergoes the orientational jump and the rest of the molecule then follows. Intuitively, this can be understood if we consider that the volume associated with backbone rotation is much larger than that associated with N*−H* rotation.

We have calculated the average number of H-bonds associated with a rotating CH_3CONH_2 molecule, the initial H-bond acceptor and the final H-bond acceptor along the average trajectory (see Figure 9). The number of H-bonds associated with the initial and the final donors is ∼2.8. Incidentally, each CH_3CONH_2 molecule offers three hydrogen bonding sites, the two amide H atoms can act as donors, whereas the carbonyl oxygen can act as an acceptor. As time proceeds, due to inherent thermal fluctuations in the system, the initial H-bond acceptor gets overcoordinated and the final H-bond acceptor becomes under-coordinated before it prepares for an orientational jump. The jump then helps release the internal stress developed due to the deviation from the average co-ordination. Figure 9 shows the time evolution of the H-bond co-ordination numbers of the initial acceptor, the final acceptor and the rotating CH_3CONH_2. One typical order parameter which is responsible for driving this microscopic transition (jump) is the difference between the coordination of the initial

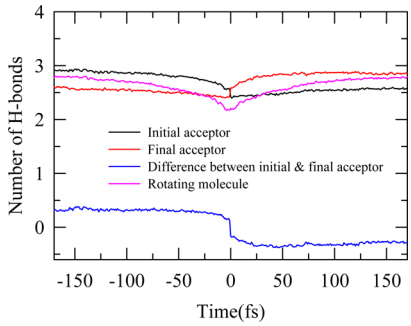

Figure 9. Time-evolution of the number of the hydrogen bonds (counting both the number of bonds donated and accepted) for the rotating molecule, the initial hydrogen bond acceptor (black curve), and the final hydrogen bond acceptor (red curve). The jump is driven by the fluctuation in the number of hydrogen bonds: the blue curve shows the difference between hydrogen bond coordination of the initial and the final hydrogen bond acceptors.

and the final H-bond acceptors. The blue curve in Figure 9 shows the time evolution of this difference, Δn_{HB}. It crosses suddenly from a positive value to a negative one at the transition state.

The above observations clearly demonstrate that orientational relaxation occurs in liquid acetamide via large amplitude jumps. This jump dynamics also affects the behavior of the experimentally accessible orientational correlation functions, $C_l(t)$. The orientational dynamics of the CH_3CONH_2 molecules has been examined via simulating the reorientational correlation functions defined as[55]

$$C_l(t) = \langle P_l|\mathbf{u}(0)\cdot\mathbf{u}(t)|\rangle / \langle P_l|\mathbf{u}(0)\cdot\mathbf{u}(0)|\rangle \quad (3)$$

where P_l denotes the Legendre polynomial of rank l and $\mathbf{u}$ is a unit vector connecting the C(−CH_3) and N(−NH_2) atoms of a given CH_3CONH_2 molecule. From Debye's model of diffusive reorientation in homogeneous media,[56,57] the l th rank correlation function can be expressed as a monoexponential function, and the corresponding reorientation time τ_l can be obtained as follows

$$\tau_l = \frac{1}{l(l+1)D_R} \quad (4)$$

where D_R is the rotational diffusion constant. For a Debye-like behavior, $\tau_1/\tau_2 \approx 3$.[56,57] Deviation from a value of 3 may be attributed to the presence of a large amplitude angular jumps.[57] Figure 10 (top panel) shows the normalized C_l (t) decays simulated for l = 1 (first rank) and 2 (second rank) associated with the backbone (connecting the C and N atoms of CH_3CONH_2). The bottom panel of Figure 10 shows the corresponding normalized C_l (t) decays for the N*−H* vector of CH_3CONH_2. Multiexponential fit parameters for these C_l (t) decays are provided in Table 1. For the backbone reorientation, the ratio between the longest time constants, $(\tau_{l=1}/\tau_{l=2})^{\text{longest}}$, has been found to be ∼1.5. For N*−H* vector, this value is ∼1.7. Such a value (deviation from three) strongly suggests presence of non-Debye reorientation mechanism which could be large amplitude angular jumps.

In Figure 11, we present the distribution of the waiting time between jumps and the time required to complete the jump (jump time). Both distributions are exponential at long times and the average time scale associated with jump (τ_{jump} ∼ 0.9 ps) is shorter compared to the average waiting time between jumps

DOI: 10.1021/jp509869d
J. Phys. Chem. B 2015, 119, 274−283

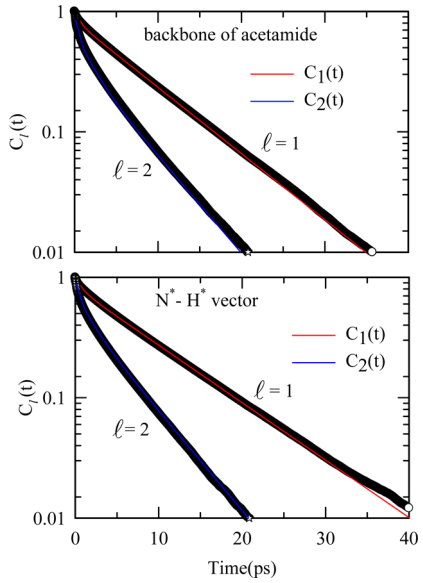

Figure 10. Simulated reorientational correlation functions of first (l = 1) and second ranks (l = 2) for molten acetamide at 368 K, and their fits. Fit parameters are given in Table 1. For discussion, see text.

Table 1. Multi-Exponential Fit Parameters for the Simulated Rank Dependent Orientational Correlation Functions at 368 K for (a) Backbone (C−N vector) and (b) N*−H* Vector

rank(l)	a_1	t_1 (ps)	a_2	t_2 (ps)	a_3	t_3 (ps)	<τ> (ps)
			(a)				
l = 1	0.17	0.63	0.83	7.9	–	–	6.7
l = 2	0.30	0.19	0.30	1.7	0.40	5.4	2.7
			(b)				
l = 1	0.18	0.8	0.82	9.1	–	–	7.6
l = 2	0.23	0.23	0.25	1.6	0.52	5.26	3.2

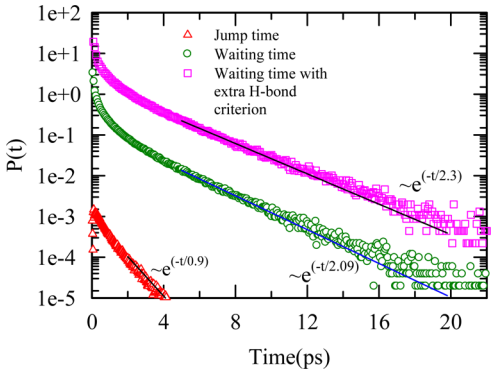

Figure 11. Distributions of waiting times between jumps (green circles and pink squares) and of the time required to complete the jump (red triangles). Both distributions are exponential at long times with the mean waiting time (2.09 ps) much longer than the mean jump time (0.9 ps). For clarity, the waiting time distribution using the additional (extra) H-bond criterion has been translated up vertically (data represented by pink squares).

(τ_{wait} ∼ 2.09 ps). Incorporation of additional hydrogen bond criterion also leads to a very similar average waiting time (τ_{wait} ∼2.3 ps). This suggests that the jumps are relatively faster events punctuated by longer periods of rest between them. It would be instructive to compare these time scales with more conventional measures of time scales of H-bond correlations.

We have calculated two well-known H-bond correlation functions $S_{HB}(t)$ and $C_{HB}(t)$. They are defined in the following way,[36−38]

$$S_{HB}(t) = \langle h(0)H(t)\rangle/\langle h\rangle \quad (5)$$

where $h(t')$ is a variable defined for a pair of CH_3CONH_2 molecules at all times, h(t′) = 1 if the pair is hydrogen bonded at time t', it is zero otherwise. $H(t)$ is a history dependent function of $h(t')$ and it is unity if $h(t')$ is continuously 1 between times t_0 and $(t_0 + t)$, where t_0 is an arbitrary origin of time. If this condition is violated, $H(t)$ is set to zero. Thus, $S_{HB}(t)$ describes the probability that a pair of CH_3CONH_2 molecules remains continuously H-bonded for a certain duration. The corresponding average relaxation time, τ_{HB}, can be treated as the average lifetime of H-bonds. Another correlation function which does not require pairs to remain H-bonded continuously, but allows them to be broken fleetingly at intermediate times, is defined below,[36,37,39,40]

$$C_{HB}(t) = \langle h(0)h(t)\rangle/\langle h\rangle \quad (6)$$

The associated average relaxation time constant, τ_{CB}, provides an estimate of the H-bond survival time. Clearly, $C_{HB}(t)$ associates with structural relaxation due to translational diffusion. The top panel of Figure 12 shows the time

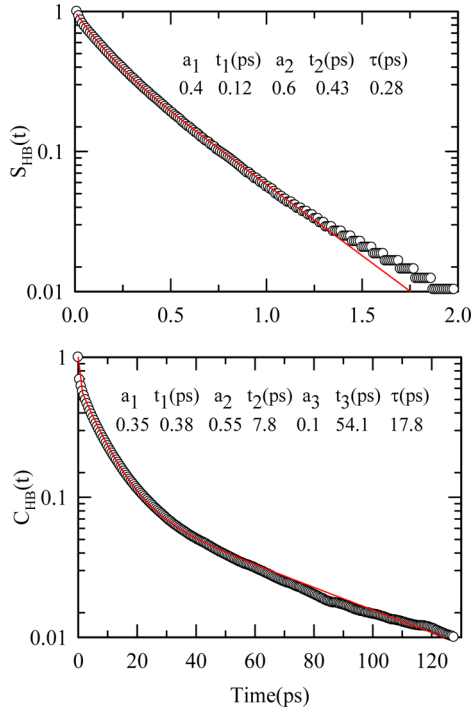

Figure 12. Simulated decay of the hydrogen bond correlation functions $S_{HB}(t)$ and $C_{HB}(t)$, defined in the text. Multiexponential function fit parameters are shown inside the panels.

dependence of $S_{HB}(t)$, whereas the bottom panel shows $C_{HB}(t)$. Multiexponential fit parameters for these simulated decays are shown inside each of these panels. The longest time scale associated with $S_{HB}(t)$ is 0.4 ps, whereas the decay of $C_{HB}(t)$ is much slower, the longest time scale being ∼54 ps. This ∼50 ps time scale is qualitatively similar to the center-of-mass translation time scale of an acetamide molecule at this temperature and suggests a connection to structural relaxation. The subpicosecond time scale is close to τ_{jump} and the other

DOI: 10.1021/jp509869d
J. Phys. Chem. B 2015, 119, 274−283

time scale (~8 ps) is close to τ_{wait} shown in Figure 11. This explains the microscopic origin for the different multi-exponential behaviors of $C_{HB}(t)$ and $S_{HB}(t)$ decays.

The free-energy profile of the average trajectory (see Figure 13), which has been discussed above, can be found by projecting the average trajectory on the free energy surface. In this calculation we have neglected the fluctuation in difference of the H-bond coordination, Δn_{HB}, a contribution, which is known to be small from similar calculations in liquid water[30,31] and have only collected the contributions arising from ΔR and θ. The value of the free energy has been arbitrarily chosen to be zero at the beginning and end of the average trajectory. The free energy barrier estimated from this free-energy profile is about 0.5 kcal/mol (~0.7 k_BT). This value is approximately one-fourth of what has been estimated for liquid water at room temperature.[30,31] This difference (from water) is expected if one considers the qualitative difference of the H-bond networks between liquid acetamide and liquid water. Figure 14 shows various sections of the free energy surface as a function of θ for different values of $\Delta R(\Delta n_{HB} = 0)$. At negative values of ΔR, the free energy has a single minimum at negative θ. This signifies that the N*–H* vector of the rotating acetamide molecule is H-bonded to its initial partner. Only when the transition state is reached ($\Delta R = 0$), the free energy section attains a symmetric double well structure (black curve in Figure 14). This feature is very similar to that observed for liquid water and emphasizes that the crossing of the barrier by angular jumps can only happen when the surrounding has prepared itself by situating the initial and the final H-bond acceptor oxygen atoms at equal distances from the nitrogen atom (N*) of the rotating acetamide molecule.

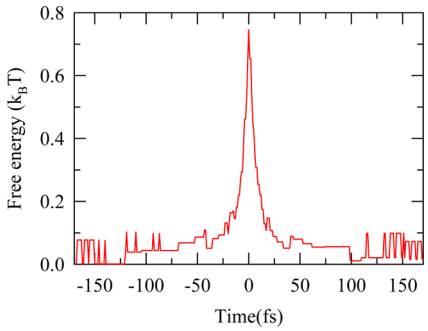

Figure 13. Free energy as a function of time along the average jump trajectory shown in Figure 5. The transition state has the highest free energy with the two stable minima on both sides of the transition state.

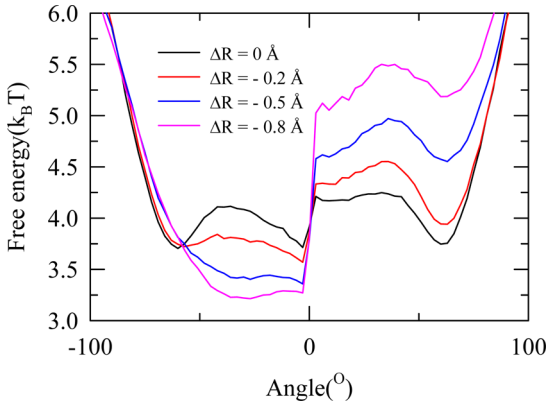

Figure 14. Cuts of the free energy surface, as a function of θ, are shown for various values of $\Delta R = (R_{N^*O_A} - R_{N^*O_B})$ and $\Delta n_{HB} = 0$. The function becomes symmetric about $\theta = 0$ for $\Delta R = 0$ (black curve). At other negative values of ΔR (red, blue, and pink curves), the cut of the free energy surface has a minima at a negative value of θ. The kinks near $\theta = 0$ are due to insufficient statistics in the close proximity to the transition state.

V. CONCLUSIONS

In summary, the present study has revealed presence of orientational jumps in molten acetamide and a significant translation-rotation coupling. The barrier to the orientation jumps has been estimated to be around 0.7 k_BT which is a factor of ~4 less than that reported for liquid water at ~300 K. The jump and waiting time distributions are exponential at long time with time constants correlating well with those obtained from continuous and structural hydrogen bond relaxation dynamics. Jump angle distributions for both the acetamide backbone and the amide vectors are asymmetric with long tails extended toward large angles. The ratios of the longest time constants associated with the first and second rank orientational correlation functions simulated for the backbone and amide vectors exhibit deviations from diffusive orientational diffusion and suggest, much like in the case of liquid water,[30,31,58] presence of angular jumps.

The interconnection between jump reorientations and H-bond dynamics can be extended to room temperature ionic liquids (RTILS) and their binary mixtures with protic solvents as they possess highly heterogeneous solution structure and exhibit nonexponential relaxation kinetics.[59−67] It would be interesting to explore how spatial heterogeneity in such systems affects the jump dynamics and H-bond relaxations and modifies the interconnection between them. Likewise, characterization of jumps and their dynamics for interfacial water confined in carbon nanotubes,[68] microemulsions[69,70] and vesicles[71] and the relationship with H-bond dynamics would be worth investigation.

■ ASSOCIATED CONTENT

Ⓢ Supporting Information

CHARMM representation of acetamide molecule and force field parameters used in our simulations. This material is available free of charge via the Internet at http://pubs.acs.org.

■ AUTHOR INFORMATION

Corresponding Authors

*(R.B.) E-mail: ranjit@bose.res.in. Fax:+91 33 2335 3477. Telephone: +91 33 2335 5706.

*(.B.M.) E-mail: biswaroop.mukherjee@gmail.com. Fax: +91 33 2335 3477. Telephone: +91 33 2335 5706.

Notes

The authors declare no competing financial interest.

■ ACKNOWLEDGMENTS

We thank anonymous reviewers for critical comments which helped improve the quality of the manuscript. S.D. acknowledges the CSIR for a research fellowship. The computational facility availed through the TUE-CMS project, SR/NM/NS-29/2011(G), is gratefully acknowledged. We also thank "Garuda" for providing computational resources at the initial stage of this work.

DOI: 10.1021/jp509869d
J. Phys. Chem. B 2015, 119, 274−283

REFERENCES

(1) Dixon, D. A.; Dobbs, K. D.; Valentini, J. J. Amide-Water and Amide-Amide Hydrogen Bond Strengths. *J. Phys. Chem.* **1994**, *51*, 13435−13439.

(2) Mitchell, J. B. O.; Price, S. L. On the electrostatic directionality of N-H···O═C hydrogen bonding. *Chem. Phys. Lett.* **1989**, *154*, 267−272.

(3) Jedlovszky, P. The local structure of various hydrogen bonded liquids: Voronoi polyhedra analysis of water, methanol, and HF. *J. Chem. Phys.* **2000**, *113*, 9113−9121.

(4) Wong, M. W.; Wiberg, K. B. Structure of Acetamide: Planar or Nonplanar. *J. Phys. Chem.* **1992**, *96*, 668−671.

(5) Ludwig, R.; Weinhold, F.; Farrar, T. C. Theoretical study of hydrogen bonding in liquid and gaseous N-methylformamide. *J. Chem. Phys.* **1997**, *107*, 499−507.

(6) Kerridge, D. H. The chemistry of molten acetamide and acetamide complexes. *Chem. Soc. Rev.* **1988**, *17*, 181−227.

(7) Stafford, O. F. Acetamide as Solvent. *J. Am. Chem. Soc.* **1933**, *55*, 3987−3988.

(8) Yntema, L. F.; Audrieth, L. F. Acetamide and Formamide as Solvents for the Electrodeposition of Metals. *J. Am. Chem. Soc.* **1930**, *52*, 2693−2698.

(9) Dawson, L. R.; Sears, P. G.; Graves, R. H. Solvents Having High Dielectric Constants. II. Solutions of Alkali Halides in *N*-Methylacetamide from 30 to 60°. *J. Am. Chem. Soc.* **1955**, *77*, 1986−1989.

(10) Wallace, R. A. Equivalent conductivity of potassium halides in molten acetamide. *J. Phys. Chem.* **1971**, *75*, 2687−2690.

(11) Nasr, S.; Ghédira, M.; Cortés, R. H-bonding in liquid acetamide as studied by x-ray scattering. *J. Chem. Phys.* **1999**, *110*, 10487−10492.

(12) Nasr, S. H-bonding in amorphous acetamide CH3CONH2 as studied by x-ray scattering. *J. Chem. Phys.* **2001**, *115*, 6569−6577.

(13) Trabelsi, S.; Nasr, S. Intermolecular association in liquid N-methylacetamide as studied by x-ray scattering. *J. Chem. Phys.* **2004**, *121*, 6380−6385.

(14) Hammami, F.; Nasr, S.; Bellissent-Funel, M.-C. Neutron scattering study of the H-bond network in amorphous N-methylformamide. *J. Chem. Phys.* **2005**, *122*, 064505/1−8.

(15) Trabelsi, S.; Bahri, M.; Nasr, S. X-ray scattering and density-functional theory calculations to study the presence of hydrogen-bonded clusters in liquid N-methylacetamide. *J. Chem. Phys.* **2005**, *122*, 024502/1−8.

(16) Kashyap, H. K.; Pradhan, T.; Biswas, R. Limiting ionic conductivity and solvation dynamics in formamide. *J. Chem. Phys.* **2006**, *125*, 174506/1−10.

(17) Pattanayak, S. K.; Prashar, N.; Chowdhuri, S. Effect of temperature and pressure on the structure, dynamics and hydrogen bond properties of liquid N-methylacetamide: A molecular dynamics study. *J. Chem. Phys.* **2011**, *134*, 154506/1−9.

(18) Biswas, R.; Bagchi, B. Solvation dynamics in slow viscous liquids: Application to amides. *J. Phys. Chem.* **1996**, *100*, 1238−1245.

(19) Biswas, R.; Das, A.; Shirota, H. Low−frequency collective dynamics in deep eutectic solvents of acetamide and electrolytes: A femtosecond Raman-induced Kerr effect spectroscopic study. *J. Chem. Phys.* **2014**, *141*, 134506.

(20) Guchhait, B.; Das, S.; Daschakraborty, S.; Biswas, R. Interaction and dynamics of (alkylamide + electrolyte) deep eutectics: Dependence on alkyl chain-length, temperature, and anion identity. *J. Chem. Phys.* **2014**, *140*, 104514/1−12.

(21) Das, A.; Das, S.; Biswas, R. Fast fluctuations in deep eutectic melts: Multi-probe fluorescence measurements and all-atom molecular dynamics simulation study. *Chem. Phys. Lett.* **2013**, *581*, 47−51.

(22) Guchhait, B.; Daschakraborty, S.; Biswas, R. Medium decoupling of dynamics at temperatures ∼100 K above glass transition temperature: A case study with (acetamide + lithium bromide/nitrate) melts. *J. Chem. Phys.* **2012**, *136*, 174503/1−16.

(23) Guchhait, B.; Gazi, H. A. R.; Kashyap, H. K.; Biswas, R. Fluorescence spectroscopic studies of (acetamide+sodium/potassium thiocyanates) molten mixtures: Composition and Temperature Dependence. *J. Phys. Chem. B* **2010**, *114*, 5066−5081.

(24) Pal, T.; Biswas, R. Heterogeneity and viscosity decoupling in (acetamide + electrolyte) molten mixtures: A model simulation study. *Chem. Phys. Lett.* **2011**, *517*, 180−185.

(25) Gazi, H. A. R.; Guchhait, B.; Daschakraborty, S.; Biswas, R. Fluorescence dynamics in supercooled (acetamide + calcium nitrate) molten mixtures. *Chem. Phys. Lett.* **2011**, *501*, 358−363.

(26) Zhang, Q.; Vigier, K. D. O.; Royer, S.; Jérôme, F. Deep eutectic solvents: synthesis, properties and applications. *Chem. Soc. Rev.* **2012**, *41*, 7108−7146.

(27) Wagle, D. V.; Zhao, H.; Baker, G. A. Deep eutectic solvents: Sustainable media for nanoscale and functional meterials. *Acc. Chem. Res.* **2014**, *47*, 2299−2308.

(28) van der Zwan, G.; Hynes, J. T. Chemical reaction rates and solvation dynamics in electrolyte solutions: ion atmosphere friction. *Chem. Phys.* **1991**, *152*, 169−183.

(29) van der Zwan, G.; Hynes, J. T. Nonequilibrium salvation dynamics in solution dynamics. *J. Chem. Phys.* **1983**, *78*, 4174−4185.

(30) Laage, D.; Hynes, J. T. A molecular jump mechanism of water reorientation. *Science* **2006**, *311*, 832−835.

(31) Laage, D.; Hynes, J. T. On The Molecular Mechanism of Water Reorientation. *J. Phys. Chem. B* **2008**, *112*, 14230−14242.

(32) Laage, D.; Hynes, J. T. Reorientional dynamics of water molecules in anionic hydration shells. *Proc. Natl. Acad. Sci. U.S.A.* **2007**, *104*, 11167−11172.

(33) Laage, D.; Stirnemann, G.; Hynes, J. T. Why Water Reorientation Slows without Iceberg Formation around Hydrophobic Solutes. *J. Phys. Chem. B* **2009**, *113*, 2428−2435.

(34) Stirnemann, G.; Hynes, J. T.; Laage, D. Water Hydrogen Bond Dynamics in Aqueous Solutions of Amphiphiles. *J. Phys. Chem. B* **2010**, *114*, 3052−3059.

(35) Laage, D.; Hynes, J. T. On the Residence Time for Water in a Solute Hydration Shell: Application to Aqueous Halide Solutions. *J. Phys. Chem. B* **2008**, *112*, 7697−7701.

(36) Rapaport, D. C. Hydrogen bonds in water. *Mol. Phys.* **1983**, *50*, 1151−1162.

(37) Chandra, A. Effects of Ion Atmosphere on Hydrogen-Bond Dynamics in Aqueous Electrolyte Solutions. *Phys. Rev. Lett.* **2000**, *85*, 768−771.

(38) Luzar, A. Resolving the hydrogen bond dynamics conundrum. *J. Chem. Phys.* **2000**, *113*, 10663−10675.

(39) Luzar, A.; Chandler, D. Hydrogen-bond kinetics in liquid water. *Nature* **1996**, *379*, 55−57.

(40) Luzar, A.; Chandler, D. Effect of environment on hydrogen bond dynamics in liquid water. *Phys. Rev. Lett.* **1996**, *76*, 928−931.

(41) Kumar, R.; Schmidt, J. R.; Skinner, J. L. Hydrogen bonding definitions and dynamics in liquid water. *J. Chem. Phys.* **2007**, *126*, 204107/1−12.

(42) Indra, S.; Biswas, R. Hydrogen-bond dynamics of water in presence of an amphiphile, tetramethylurea: signature of confinement-induced effects. *Mol. Simul.* **2014**, DOI: 10.1080/08927022.2014.965705.

(43) Mitchell, J. A.; Reid, E. E. The Preparation of Aliphatic Amides. *J. Am. Chem. Soc.* **1931**, *53*, 1879−1883.

(44) Smith, W.; Forster, T. R. The DL_POLY Molecular Simulation Package, Daresbury Laboratory: Cheshire, U.K., 1999.

(45) Habasaki, J.; Nagi, K. L. Heterogeneous dynamics of ionic liquids from molecular dynamics simulations. *J. Chem. Phys.* **2008**, *129*, 194501/1−15.

(46) MacKerell, A. D., Jr.; Wiorkiewicz-Kuczera, J.; Karplus, M. An all-atom empirical energy function for the simulation of nucleic acids. *J. Am. Chem. Soc.* **1995**, *117*, 11946−11975.

(47) Yong, C. W. *DL_FIELD*; STFC Daresbury Laboratory: Cheshire, U.K., 2011 http://www.cse.scitech.ac.uk/ccg/software/DL_FIELD.

(48) Allen, M. P.; Tildesley, D. J. *Comput. Simulations Liq.*; Oxford University Press: New York, 1987.

(49) Martinez, L.; Andrade, R.; Birgin, E. G.; Martinez, J. M. Packmol: A package for building initial configurations for molecular dynamics simulations. *J. Comput. Chem.* **2009**, *30*, 2157−2164.

DOI: 10.1021/jp509869d
J. Phys. Chem. B 2015, 119, 274−283

(50) http://en.wikipedia.org/wiki/Acetamide.
(51) Nose, S. A unified formulation of the constant temperature molecular dynamics methods. *J. Chem. Phys.* **1984**, *81*, 511−519.
(52) Hoover, W. G. Canonical dynamics: Equilibrium phase-space distributions. *Phys. Rev. A* **1985**, *31*, 1695−1697.
(53) Laage, D.; Hynes, J. T. Do more strongly hydrogen-bonded water molecules reorient more slowly? *Chem. Phys. Lett.* **2006**, *433*, 80−85.
(54) Taylor, R.; Kennard, O.; Versichel, W. Geometry of the N-H—O═C Hydrogen Bond. 2. Three-Center ("Bifurcated") and Four-Center ("Trifurcated") Bonds. *J. Am. Chem. Soc.* **1984**, *106*, 244−248.
(55) Hansen, J. P.; McDonald, I. R. *Theory of simple liquids*, 3rd ed., Academic: San Diego, 2006.
(56) Debye, P. *Polar Molecules*; The Chemical Catalog Company: New York, 1929.
(57) Seki, K.; Bagchi, B.; Tachiya, M. Orientational relaxation in a dispersive dynamic medium: Generalization of the Kubo-Ivanov-Anderson jump-diffusion model to include fractional environmental dynamics. *Phys. Rev. E* **2008**, *77*, 031505/1−10.
(58) Ludwig, R. The mechanism of the molecular reorientation in water. *ChemPhysChem* **2007**, *8*, 44−46.
(59) Pal, T.; Biswas, R. Slow solvation in ionic liquids: Connections to non-Gaussian moves and multi-point correlations. *J. Chem. Phys.* **2014**, *141*, 104501/1−12.
(60) Pal, T.; Biswas, R. Rank dependent orientational relaxation in an ionic liquid: an all-atom simulation study. *Theor. Chem. Acc.* **2013**, *132*, 1348/1−12.
(61) Daschakraborty, S.; Biswas, R. Dielectric relaxation in ionic liquids: Role of ion-ion and ion-dipole interactions, and effects of heterogeneity. *J. Chem. Phys.* **2014**, *140*, 014504/1−11.
(62) Daschakraborty, S.; Pal, T.; Biswas, R. Stokes shift dynamics of ionic liquids: Solute probe dependence, and effects of self-motion, dielectric relaxation frequency window, and collective intermolecular solvent modes. *J. Chem. Phys.* **2013**, *139*, 164503/1−12.
(63) Daschakraborty, S.; Biswas, R. Ultrafast solvation response in room temperature ionic liquids: Possible origin and importance of the collective and the nearest neighbour solvent modes. *J. Chem. Phys.* **2012**, *137*, 114501/1−11.
(64) Daschakraborty, S.; Biswas, R. Composition dependent Stokes shift dynamics in binary mixtures of 1-butyl-3-methylimidazolium tetrafluoroborate with water and acetonitrile: Quantitative comparison between theory and complete measurements. *J. Phys. Chem. B* **2014**, *118*, 1327−1339.
(65) Daschakraborty, S.; Biswas, R. Stokes shift dynamics in (ionic liquid + polar solvent) binary mixtures: composition dependence. *J. Phys. Chem. B* **2011**, *115*, 4011−4024.
(66) Pal, T.; Biswas, R. Stokes shift dynamics in (non-dipolar ionic liquid + dipolar solvent) binary mixtures: A semi-molecular theory. *J. Chem. Phys.* **2014**, *141*, 164502/1−10.
(67) Barra, K. M.; Sabatini, R. P.; McAtee, Z. P.; Heitz, M. P. Solvation and rotation dynamics in the trihexyl(tetradecyl)-phosphonium chloride ionic liquid/methanol cosolvent system. *J. Phys. Chem. B* **2014**, *118*, 12979−12992.
(68) Mukherjee, B.; Maiti, P. K.; Dasgupta, C.; Sood, A. K. Jump Reorientation of Water Molecules Confined in Narrow Carbon Nanotubes. *J. Phys. Chem. B* **2009**, *113*, 10322−10330.
(69) Guchhait, B.; Biswas, R.; Ghorai, P. Solute and solvent dynamics in confined equal-sized aqueous environments of charged and neutral reverse micelles: A combined dynamic fluorescence and all-atom molecular dynamics simulation study. *J. Phys. Chem. B* **2013**, *117*, 3345−3361.
(70) Biswas, R.; Das, A. R.; Pradhan, T.; Touraud, D.; Kunz, W.; Mahiuddin, S. Spectroscopic studies of catanionic reverse micro-emulsion: correlation with the superactivity of horseradish peroxidase enzyme in a restricted environment. *J. Phys. Chem. B* **2008**, *112*, 6620−6628.
(71) Sarma, N.; Borah, J. M.; Mahiuddin, S.; Gazi, H. A. R.; Guchhait, B.; Biswas, R. Influence of chain length of alcohols on Stokes shift dynamics in catanionic vesicles. *J. Phys. Chem. B* **2011**, *115*, 9040−9049.

DOI: 10.1021/jp509869d
J. Phys. Chem. B 2015, 119, 274−283